ELSEVIER

Polymer 40 (1999) 6125–6134

polymer

Miscibility, phase behavior, and Curie transition in blends of vinylidene fluoride/trifluoroethylene copolymer and Poly(1,4-butylene adipate)

Kap Jin Kim[1], Thein Kyu*

Institute of Polymer Engineering, The University of Akron, Akron, OH 44325, USA

Received 15 May 1998; received in revised form 13 November 1998; accepted 17 November 1998

Abstract

The phase diagram and Curie transition behavior in binary crystalline polymer blends of poly(vinylidene fluoride-trifluoethylene) P(VDF/TrFE) and poly(1,4-butylene adipate) (PBA) were investigated using differential scanning calorimetry, light scattering, and infrared spectroscopy. In order of descending temperature, the phase diagram exhibits a lower critical solution temperature (LCST), two crystal melting transitions, a paraelectric-ferroelectric phase transition, and a single glass transition. Liquid–liquid phase separation is observed at approximately 50°C higher than the melting points of P(VDF/TrFE) in the blends with PBA. The cloud point phase diagram is thermally reversible as typical for a true LCST. Increasing PBA concentration results in depression of the melting point of P(VDF/TrFE) in the blends. The analysis based on the melting point depression of P(VDF/TrFE) and PBA gives $\chi_{12} = -0.592$ at 160°C and -0.071 at 61°C, respectively. Based on the shift of the C = O absorption peak, the origin of miscibility in this blend was attributed to specific interactions between the CH_2 and/or CF_2 sites of P(VDF/TrFE) and the C = O groups of PBA. The isothermal and non-isothermal crystallization behavior of P(VDF/TrFE) in the blends was analyzed in relation to the behavior of the ferroelectric-paraelectric phase transition, often known as the 'Curie transition'. It was found that the addition of PBA (up to 70 wt%) increases the enthalpy of the Curie transition as well as the temperature of the Curie transition. Of particular interest is the possible formation of a ferroelectric phase directly from the melt without passing through the paraelectric phase in the high PBA compositions.

Keywords: VDF/TrFE copolymer; Poly(1,4-butylene adipate); Blend miscibility

1. Introduction

Miscibility, phase behavior, crystallization kinetics, and phase transformation in blends of poly(vinylidene fluoride)(PVDF) with various ester containing polymers were extensively investigated because of a rich variety of crystalline morphology of the PVDF and its ability to form miscible blends with ester containing polymers [1–9], including poly(methyl methacrylate) (PMMA), poly(methyl acrylate) (PMA), and poly(vinyl acetate) (PVAc). These ester containing polymers are miscible with PVDF because of their specific pendant carbonyl sites capable of forming hydrogen bonding or exerting dipole–dipole interaction with the CH_2 or CF_2 groups of PVDF. Especially PVDF/PMMA and PVDF/PVAc blends are known to be completely miscible in the amorphous state and the mixtures exhibit a lower critical solution temperature (LCST) above the melting temperature of PVDF [1,2]. The copolymer of vinylidene fluoride and trifluoroethylene, hereafter abbreviated as P(VDF/TrFE), is found to be miscible with PMMA and PVAc [10,11], even though it shows a smaller negative value of the interaction parameter relative to those of the corresponding PVDF blends resulting from the reduced net polarity in the P(VDF/TrFE) copolymer.

PVDF is also known to be partially miscible in the amorphous state with some semicrystalline polymers containing carbonyl groups in their backbone chains such as poly(ϵ-caprolactone) (PCL) [12], poly(pivalolactone) (PPVL) [13], and poly(1,4-butylene adipate) (PBA) [14–17]. The primary reason for their partial miscibility (or the limited miscibility gap) may be ascribed to a specific interaction between fluorocarbon and ester groups of the constituents. However, this kind of specific interaction weakens at elevated temperatures above the crystal melting temperature of PVDF, resulting in liquid–liquid phase separation. During cooling, the phase behavior becomes extremely complex as crystallization of one or both components competes with

* Corresponding author. Tel.: +1-330-972-6672; fax: +1-330-258-2339.

E-mail address: tkyu@uakron.edu (T. Kyu)

[1] Permanent address: Department of Textile Engineering, Kyung Hee University, 1 Seochun-ri, Kiheung-eup, Yongin-si, Kyunggi-do 449-701, South Korea.

0032-3861/99/$ - see front matter
PII: S0032-3861(98)00825-8

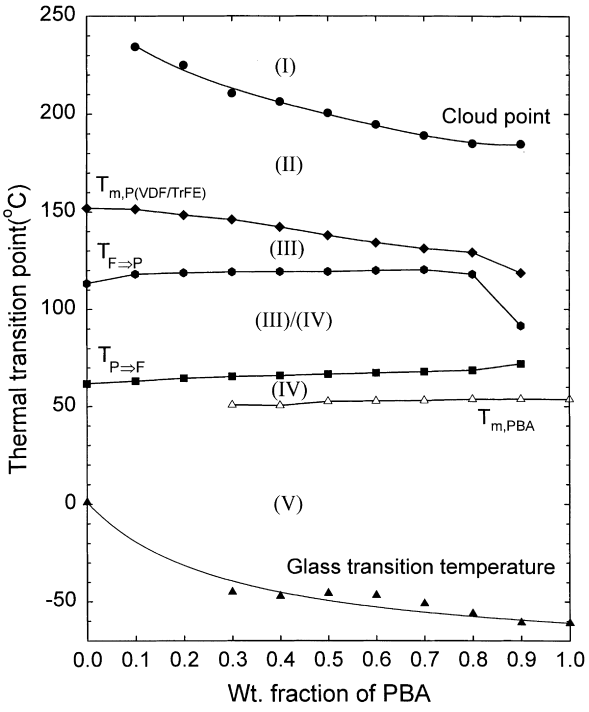

Fig. 1. Phase diagram of P(VDF/TrFE)/PBA blends showing (A) cloud point curve; (B) melting temperature of P(VDF/TrFE); (C) paraelectric-to-ferroelectric transition temperature of P(VDF/TrFE); (D) ferroelectric-to-paraelectric transition temperature of P(VDF/TrFE); (E) melting temperature of PBA; and (F) glass transition temperature.

phase separation. In most cases, two distinct crystalline phases coexist with a single amorphous phase or with two segregated amorphous phases.

Recently, Manley and co-workers [14–17] reported on miscibility, phase diagram, and crystallization behavior of a semicrystalline/semicrystalline polymer blend, viz., PVDF/PBA. The choice of their blend system has several advantages over other PVDF/semicrystalline polymer blends. First, the melting points of the constituents are about 100°C apart, hence the melting and crystallization behavior occurring in both PVDF and PBA could be studied separately. Second, the observed LCST is located at ~ 60°C above the melting temperature of the PVDF crystals, therefore the liquid–liquid phase separation behavior could also be studied without any interference from the melting transitions. In the PVDF/PCL blend, the LCST coexistence curve overlaps with the melting and/or crystallization curves over a wide composition range, thus phase separation and crystallization interfere mutually [12]. In the case of PVDF/PPVL blends [13], the LCST curve is located at extremely high temperatures, therefore thermal degradation may have occurred during the liquid–liquid phase separation.

In addition to the crystallization/melting transitions, the random copolymers of VDF/TrFE display a Curie transition in which the ferroelectric phase transforms to a paraelectric phase. The Curie transition behavior of the P(VDF/TrFE) copolymer is affected by many factors such as VDF content, external electric field, poling, hydrostatic pressure leading to different crystal forms, internal stress, crystallinity, and annealing conditions, etc. [18–21]. Even though there were numerous reports on the Curie transition of the VDF copolymers, only one paper dealt with the Curie transition behavior of the blend of P(VDF/TrFE) and PMMA [18]. To date, the blends of P(VDF/TrFE) with other crystalline polymers remain an unexplored area. Since PVDF is shown to be miscible with PBA [14–17], one can anticipate that P(VDF/TrFE) would also be miscible with PBA. In the P(VDF/TrFE)/PBA blend, the phase behavior is expected to be more complex than in the PVDF/PBA blend because of the existence of Curie transition in the copolymer. In this study, the emphasis is placed on establishment of the phase diagram, determination of miscibility, and investigation of the influence of blending on the crystallization and Curie transition behavior of the P(VDF/TrFE)/PBA blend using Fourier transformed infrared spectroscopy (FTIR), differential scanning calorimetry (DSC), and cloud point methods.

2. Experimental

The P(VDF/TrFE) copolymer with a molar ratio of 75/25 was kindly supplied by Atochem Co. in a chip form, and was used as-received. Its molecular weight was not determined. The PBA sample with a weight-averaged molecular weight (M_w) of 12 000 was purchased from Scientific Polymer Products, Inc. and used without further purification. P(VDF/TrFE) and PBA were dissolved separately in acetone. The 4% acetone stock solutions were subsequently mixed in the desired proportions. Film samples were cast on a Petri-dish for DSC, glass slide for light scattering, or potassium bromide (KBr) window for Fourier transformed infrared (FTIR) spectroscopic studies. The solvent was allowed to evaporate on a hot plate maintained at 50°C for 30 min and the resulting films were further dried in vacuum at 80°C for 3 days. In this way, blend samples were prepared in various compositions ranging from 90/10 to 10/90 ratio by weight with 10% increment; the first numeral refers to P(VDF/TrFE).

The IR absorbance spectra of the blends were recorded as a function of temperature on a Perkin–Elmer (Model 16PC FTIR) spectrometer equipped with a custom designed heating cell. The spectra were acquired from 4200 to 450 cm^{-1} with a resolution of 2 cm^{-1} by averaging 32 scans under nitrogen circulation. For quantitative analysis, the films used in IR measurements were adjusted sufficiently thin to obey the Beer–Lambert law.

Non-isothermal crystallization, melting, and Curie transitions of the blends were determined using a Perkin–Elmer DSC-7. At the beginning of each experiment, the sample was heated at 180°C for 10 min to remove its initial thermal history. DSC thermograms were scanned from 180°C to −20°C to cover melting, crystallization, and paraelectric-to-ferroelectric phase transition of the P(VDF/TrFE) constituent and the melting and crystallization of the PBA

part. The heating and cooling rates were 20 and 5°C/min, respectively. The glass transition temperatures of the quenched blends were determined on a Du Pont DSC-9000 from −100°C to 180°C at 20°C/min. Indium standard was used for calibration of temperature and enthalpy.

Cloud point measurements were undertaken on the P(VDF/TrFE)/PBA blends in the melt state by measuring the scattering intensity at $\theta = 10^{\circ}$ during heating at a heating rate of 0.5°C/min. An abrupt change in the scattered intensity during phase separation was regarded as a cloud point.

3. Results and discussion

3.1. Phase behavior

The overall phase diagram of the P(VDF/TrFE)/PBA blend system is depicted in Fig. 1. In order of ascending temperature, the pure PBA reveals only two phase transitions, i.e. glass transition (T_g) and melting (T_m), whereas the neat P(VDF/TrFE) copolymer shows three phase transitions, i.e. glass transition, melting, and Curie transition. The Curie phase transition occurs reversibly from paraelectric-to-ferroelectric ($T_{P\Rightarrow F}$) during cooling, and vice versa ferroelectric-to-paraelectric transition ($T_{F\Rightarrow P}$) during heating. The intermediate mixtures undergo more complex phase transitions, showing a single glass transition, two melting transitions, Curie transition, and liquid–liquid phase separation above the lower critical solution temperature (LCST). P(VDF/TrFE) and PBA are apparently miscible in a temperature gap between the melting curve of P(VDF/TrFE) and the LCST. Raising the temperature of the blend from a single phase (region II) to an immiscible gap (region I) eventually leads to liquid–liquid phase separation associated with the reduction of the specific interaction between the polar groups of the constituents. The fact that the LCST minimum is located at an extremely high PBA composition (> 90% PBA) implies that the molecular weight of the P(VDF/TrFE) must be significantly higher than that of the PBA. Upon lowering the temperature from region II (single phase) to region III, denoted by $T_{P\Rightarrow F} < T < T_{m,P(VDF/TrFE)}$, the P(VDF/TrFE) component in the blends crystallizes into a paraelectric crystalline phase. The non-crystalline P(VDF/TrFE) along with amorphous PBA must be rejected from the crystallizing fronts of the P(VDF/TrFE) crystallites, thereby forming a coexistence two-phase region consisting of a single phase blend of amorphous PBA/amorphous P(VDF/TrFE) and the paraelectric crystalline phase (region III). Further cooling to region IV, $T_{m,PBA} < T < T_{P\Rightarrow F}$ transforms the paraelectric crystalline phase into the ferroelectric crystalline phase, thus the amorphous P(VDF/TrFE)/amorphous PBA mixture is expected to remain in a single phase as revealed by a single glass transition. Hence, region IV appears to be characterized by the coexistence of the mixed amorphous P(VDF/TrFE)/PBA phase and the ferroelectric crystalline phase [22]. Lowering the temperature below T_m of PBA (i.e., $T < T_{m,PBA}$) drives the amorphous PBA to crystallize, leading to a three-phase morphology in which two distinct crystalline structures coexist with a single amorphous blend. Since P(VDF/TrFE) having more than 60 mol% of VDF undergoes a first order phase transition, a large hysteresis is generally observed in the Curie transition [23]. In the present study, the Curie transition ($T_{F\Rightarrow P}$) during heating is approximately 50°C higher than that ($T_{P\Rightarrow F}$) during cooling for the pure P(VDF/TrFE). The P(VDF/TrFE) blends containing <90 wt% PBA show a comparable hysteresis in the Curie transition.

3.2. Melting transitions

As evident in Fig. 1, the melting point of P(VDF/TrFE) is lowered with increasing PBA concentration. It should be pointed out that the above melting points are, by no means equilibrium values. In principle, the occurrence of the melting-point depression depends not only on thermodynamic interaction, but also on crystalline morphology. The presence of a paraelectric phase makes the determination of equilibrium melting temperatures very difficult. The melting point depression of a miscible amorphous/crystalline polymer mixture is customarily analyzed in accordance with the Nishi–Wang's approach [24] as follow:

$$\frac{1}{T_m^o(\phi_1)} - \frac{1}{T_m^o} = -\frac{RV_{2u}}{\Delta h_{2u} V_{1u}}\left[\frac{\ln(1-\phi_1)}{m_2} + \left(\frac{1}{m_2} - \frac{1}{m_1}\right)\phi_1 + \chi_{12}\phi_1^2\right] \quad (1)$$

where T_m^o and $T_m^o(\phi_1)$ represent the equilibrium melting temperatures of the crystalline polymer in the neat state and in the blend, respectively. ϕ_i, V_{iu}, and m_i are the volume fraction, the molar volume of the repeat unit, and the degree of polymerization of polymer i, respectively. Δh_{2u} is the heat of fusion per mole of the repeat unit of crystalline polymer 2, χ_{12} the Flory–Huggins interaction parameter, and R universal gas constant. Since P(VDF/TrFE) crystals melt well above the T_m of PBA, the PBA melt acts like diluent, thereby lowering the melting of P(VDF/TrFE) crystals in this blend. Here, subscripts 1 and 2 refer to the amorphous PBA and the crystalline P(VDF/TrFE) polymers, respectively.

For $m_1 \gg 1$ the combinatorial term in Eq. (1) can be neglected and the equation reduces to

$$\frac{1}{T_m^o(\phi_1)} - \frac{1}{T_m^o} = -\frac{RV_{2u}}{\Delta h_{2u} V_{1u}}\chi_{12}\phi_1^2 \quad (2)$$

Although the determination of equilibrium melting point of each blend according to the Hoffman–Weeks plot [25] is a preferred methodology, the Curie transition from ferroelectric-paraelectric phase transition makes such analysis extremely difficult, particularly to remove the morphological effect. Hence, the non-equilibrium melting temperature

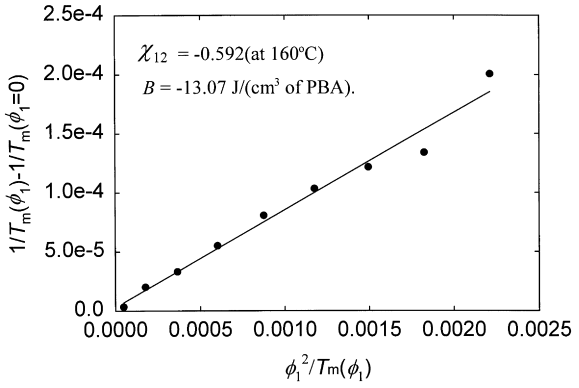

Fig. 2. Plot of melting point depression of P(VDF/TrFE) versus blend composition according to Eq. (6).

was determined from the melting endotherm obtained during heating at 20°C/min for each blend crystallized by cooling non-isothermally from the melt to −20°C at 5°C/min. In practice, polymer crystals grow and melt under non-equilibrium conditions, thus the melting temperature for a crystal of thickness l may be expressed in terms of the well-known Thompson–Gibbs equation

$$T_m(l) = T_m^o\left(1 - \frac{2\sigma_e}{\Delta h_{2u}^l}\right) \tag{3}$$

where σ_e is the surface free energy per unit area of the fold surface in the chain-folded lamellar crystal and $\Delta h'_{2u}$ is the heat of fusion per unit volume of crystal. Now, if one assumes that $T_m^o(\phi_1)$ is lowered by a factor given in Eq. (3) and it can be rewritten as

$$\left(1 - \frac{2\sigma_e}{\Delta h_{2u}^l(\phi_1)}\right)\frac{1}{T_m(\phi_1)} = \frac{1}{T_m^o} - \frac{R}{\Delta h_{2u}^V 1u}\chi_{12}\phi_1^2 \tag{4}$$

However, Liu and co-workers [17] recently reported that the thickness of PVDF lamella is nearly constant for all blend compositions when the PVDF/PBA blends were quenched from the melt to room temperature at the same condition. On the assumption that their result for the PVDF is applicable to the present P(VDF/TrFE)/PBA blend system, $l(\phi_1) = l(\phi_1 = 0)$, one obtains

$$\frac{T_m(\phi_1 = 0)}{T_m^o} = \left(1 - \frac{2\sigma_e}{\Delta h_{2u}^l(\phi_1 = 0)}\right) \tag{5}$$

Inserting Eq. (5) and $\chi_{12} = BV_{1u}/(RT)$ into Eq. (4) leads to

$$\frac{1}{T_m(\phi_1)} - \frac{1}{T_m(\phi_1 = 0)} = -\frac{BT_m^o}{\Delta h_{2u}^T \mathrm{m}(\phi_1 = 0)} \cdot \frac{\phi_1^2}{T_m(\phi_1)} \tag{6}$$

where B is the interaction energy density.

The plot of melting point depression versus blend composition:

$$\frac{1}{T_m(\phi_1)} - \frac{1}{T_m(\phi_1 = 0)} \text{ against } \frac{\phi_1^2}{T_m(\phi_1)}$$

is depicted in Fig. 2, showing a reasonably good linear relation, implying that the dependence of interaction parameter χ_{12} and lamellar thickness on composition may be insignificant in the present case. Now, from the slope of this linear plot, B and χ_{12} were determined. Using all parameters listed in Table 1, one obtains $\chi_{12} = -0.592$ (at 160°C) and $B = -13.07$ J/cm^3 of PBA.

In view of the fact that the net polarity of P(VDF/TrFE) and the LCST (ca. 200°C at the 50/50 composition) in the P(VDF/TrFE)/PBA system are lower than those in the PVDF/PBA system (ca. 235°C at the 50/50 composition), the χ_{12} value of the P(VDF/TrFE)/PBA blend is expected to be smaller than that of the PVDF/PBA blend [14]. Contrary to our expectation, the negative χ_{12} value turned out to be very large. One speculation is that an increase of CF groups, i.e. the increase in the number of interacting sites (CF groups) with the ester group (PBA) rather than the net polarity itself is responsible for this enhanced miscibility. Nevertheless, there is no doubt that the large negative value of χ_{12} at 160°C indicates intimate miscibility of the P(VDF/TrFE)/PBA polymer pair, forming a single phase mixture in the melt state between the LCST and the melting temperature similar to the case of the PVDF/PBA blend [14].

In the vicinity of crystal melting of PBA, a small but definitive depression of the T_m of PBA was observed in the blends with P(VDF/TrFE). In the PBA crystal melting region, the P(VDF/TrFE) crystals may not contribute to the depression of PBA melting. So only the amorphous fractions of the P(VDF/TrFE), as determined from the crystallinity derived from the DSC results (Fig. 6), were used in the calculation. From the analysis of this T_m depression, the χ_{12} value was estimated to be −0.071 at 61°C. This reduction in miscibility between P(VDF/TrFE) and PBA at a lower temperature will be discussed in a later section.

Table 1
Values of all parameters used in the calculation of the interaction density B and parameter χ_{12}

Density of PBA	1.23 g/cm^3 [14]
Density of P(VDF/TrFE)	1.8455 g/cm^3 [10]
V_{1u}	162.776 cm^3/mol [14]
V_{2u}	37.135 m^3/mol [10]
Δh_{1u}	21481.5 J/mol [14]
Δh_{1u}	132.0 J/cm^3 [14]
Δh_{2u}	5985 J/mol [10]
Δh_{2u}	160.71 J/cm^3 [10]
T_m^o of P(VDF/TrFE)	431.2 K [10]
$T_m(\phi_1 = 0)$ of P(VDF/TrFE)	425.18 K
$T_{m,PBA}^o$	334 K [10]
$T_{m,PBA}(\phi_2 = 0)$	327 K

3.3. Specific interactions

The fact that the interaction parameter χ_{12} calculated from the melting point depression of P(VDF/TrFE) has a large negative value implies that there is a specific interaction between PBA and P(VDF/TrFE) such as hydrogen

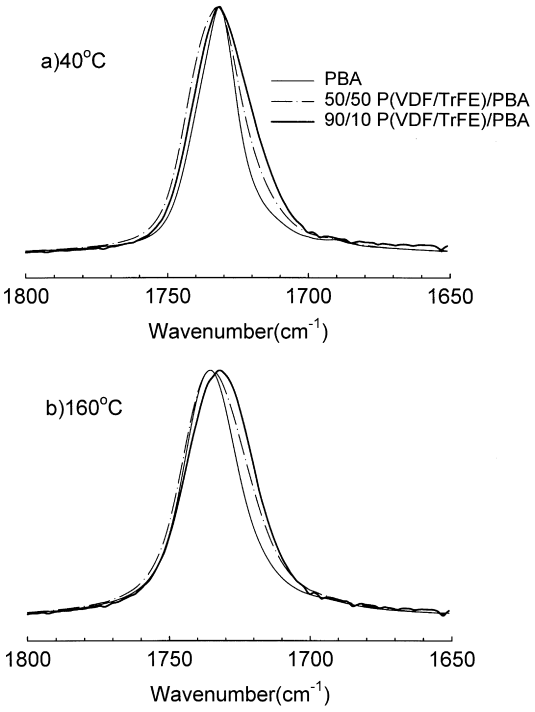

Fig. 3. Absorbance IR spectra of various P(VDF/TrFE)/PBA blends at: (a) 40°C; and (b) 160°C.

bonding and/or dipole–dipole interaction. The specific interaction between the C = O and CF (or CH_2) groups is one of the major contributors to miscibility in the blend of the PVDF/ or P(VDF/TrFE)/vinyl polymers having pendant carbonyl groups [5,6,7,9,10]. This can be verified in terms of the frequency shift of the stretching vibration of C = O to lower frequencies, which is caused by the reduction in the force constant of C = O associated with hydrogen bonding or dipole–dipole interaction. Moreover, the magnitude of the frequency shift can be used in evaluating the level of specific interaction between the two polymers. Even though the miscibility in the blends of PVDF/polyester or P(VDF/TrFE)/polyester having the carbonyl group in the backbone is explicable by the same mechanism, the number of papers treating this mechanism for the PVDF/polyester system is limited. Based on the small frequency shift of the C = O stretching band to the lower frequency region, Penning and Manley [14] concluded that the miscibility of the PVDF/PBA system arises from the dipole–dipole interaction between the C = O and CF groups rather than the hydrogen bonding between the C = O and CH_2 groups.

It is well established that the extent of frequency shift in the C = O stretching band to lower frequencies is proportional to the number fraction of the C = O groups participating in the specific interaction with CF_2 or CH_2 group of P(VDF/TrFE). The specific interaction in the blend can be evaluated by examining the changes in the peak position and the line shape of the C = O stretching band of PBA at various blend compositions. The IR absorbance spectra recorded at 40°C and 160°C are shown in Figs. 3(a) and (b), respectively. At 40°C, both PBA and P(VDF/TrFE) are crystalline, so the amount of miscible part, i.e. amorphous P(VDF/TrFE) and amorphous PBA chains, would be relatively low. Therefore, the frequency shift of the C = O stretching band is negligibly small upon addition of P(VDF/TrFE). However, the peak broadens while skewing towards the lower frequencies, which implies that the amorphous PBA could be miscible with the amorphous P(VDF/TrFE) at 40°C. With increasing P(VDF/TrFE), the movement of the C = O peak is small (i.e. $\Delta\overline{\nu} = 3\ \mathrm{cm}^{-1}$), but it is definitely discernible at 160°C. In view of the large negative interaction parameter along with the observed peak broadening and shifting of the C = O band, PBA and P(VDF/TrFE) must be intimately mixed in the melt (160°C) [Fig. 3(b)]. This small frequency shift implies that the specific interaction between PBA and P(VDF/TrFE) may be associated with relatively weak hydrogen bonding and/or dipole–dipole interaction as in the case of the PVDF/PBA blend systems [14].

In principle, the dependence of the peak position of the C = O stretching band on temperature could be correlated with changes in the intermolecular interaction. However, the P(VDF/TrFE)/PBA system shows no drastic frequency shift with blend composition or temperature. Hence, the peak position was used as a mean value of the absorbance curve of the C = O stretching band in the range from 1780 to 1700 cm^{-1}.

$$\text{Peak position of } \overline{\nu}_{C=O} = \langle\overline{\nu}_{C=O}\rangle = \frac{\sum_i \overline{\nu}_i A_i}{\sum_i A_i} \tag{7}$$

Fig. 4 depicts the change in peak position of $\overline{\nu}_{C=O}$ as a function of temperature for various P(VDF/TrFE)/PBA blends. In the whole temperature range, the C = O peak frequency is lowered with the addition of P(VDF/TrFE) resulting from an increasing number of C = O groups of PBA interacting with the CF and/or CF_2 of P(VDF/TrFE). For the pure PBA sample, the PBA crystals melt in the vicinity of 50°C ~ 60°C, causing the C = O peak to move noticeably to a higher wavenumber which is the intrinsic characteristic of the pure PBA. However, in the range of 60°C to 90°C, the band shift for the blends with more than 50% P(VDF/TrFE) is less pronounced relative to that for the pure PBA. This implies that the number fraction of C = O groups of the PBA interacting with the amorphous P(VDF/TrFE) has increased because of the melting of the crystalline PBA phase. The peak shift suddenly becomes more drastic again in the vicinity of 100°C to 120°C upon heating, particularly at high P(VDF/TrFE) compositions. This suggests that the amorphous P(VDF/TrFE) in the as-cast blend sample is cold-crystallized into the paraelectric phase, which induces the phase separation of the melt PBA phase from the crystalline paraelectric phase of P(VDF/TrFE). This leads to the peak shift of the C = O band to a higher frequency. In view of the shift of the C = O absorption peak,

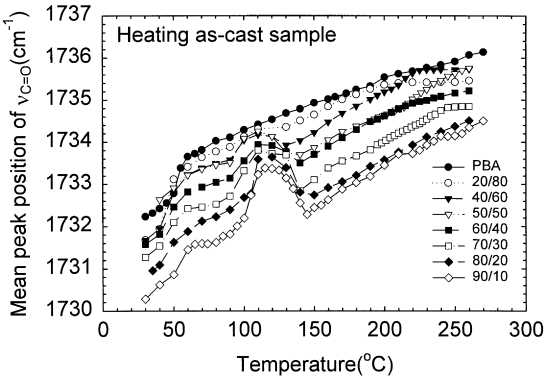

Fig. 4. Variation of the $\bar{\nu}_{C=O}$ peak versus temperature for various P(VDF/TrFE)/PBA blends.

it is reasonable to infer that the specific interactions between the CH_2 and/or CF_2 sites of P(VDF/TrFE) and the C = O groups of PBA may be responsible for the miscibility in this P(VDF/TRFE)/PBA blend system.

3.4. Glass transitions

The previously mentioned melting point depression and the IR spectroscopic analyses suggest that the P(VDF/TrFE)/PBA blend is miscible. It is natural to anticipate a single glass transition in the DSC runs, unless there exists an upper critical solution temperature below the crystallization temperatures. The glass transition temperatures (T_g) of various blends were determined from the midpoint of the transitional interval in the DSC curve measured on the melt-quenched samples. The quenching technique was adopted to minimize crystallinity of each component even though one cannot remove them completely. The T_gs of the neat P(VDF/TrFE) and PBA were located at around 0 and −61°C, respectively (Fig. 1). As expected, a single T_g was seen in the PBA-rich compositions moving slightly with increasing P(VDF/TrFE). However, the DSC T_g signal was not clearly discernible in the P(VDF/TrFE)-rich blends because of the interference of the PBA melting. The presence of crystals, although they perturb the miscibility of the amorphous phase of the two crystallizable polymers, may not be involved directly in the mixing of the amorphous chains that contributes to the T_g shift. Hence, the T_g should be plotted against the weight fraction of each amorphous phase rather than the feed ratio. The actual composition of the amorphous PBA phase was calculated from the melting enthalpy of the DSC curve measured upon heating immediately after T_g measurement. The actual composition of the amorphous P(VDF/TrFE) phase was estimated from the melt-crystallization enthalpy during cooling, as the Curie transition curve tends to overlap with the melting transition of PBA.

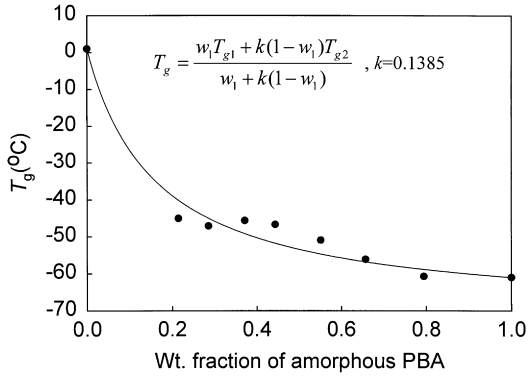

Fig. 5. Plots of the glass transition temperature versus weight fraction of the amorphous PBA phase in comparison with the prediction of the Gordon–Taylor equation.

The T_g is plotted again versus weight fraction of the amorphous PBA phase as shown in Fig. 5. It is apparent that a single T_g is observable in the blends rich in PBA. It seems that the blend miscibility at 61°C is reduced relative to that from the melting point depression of P(VDF/TrFE) at 160°C. In general, the experimental T_g curve may be analyzed using the classical Gordon–Taylor equation [26]

$$T_g = \frac{w_1 T_{g1} + k(1 - w_1)T_{g2}}{w_1 + k(1 - w_1)} \tag{8}$$

where w_1 is the weight fraction of PBA in the amorphous state, k is a G–T parameter and T_{g1} and T_{g2} are the glass transition temperatures of PBA and P(VDF/TrFE), respectively. A value of k close to unity is regarded as a signature of miscibility and is thus often used as a rough evidence of polymer blend miscibility. A value of $k = 0.1385$ gives the best curve fit, represented by the solid line in Fig. 5, which suggests limited miscibility in the range of $T < T_{m,PBA}$. This reduced miscibility as observed in the glass transition behavior is consistent with the inference obtained by the smaller negative value of the interaction parameter (−0.071 at −61°C) calculated from the melting point depression of PBA with the addition of P(VDF/TrFE). Even though the origin of the reduced miscibility in the very low temperature region has yet to be identified, it is tempting to speculate that the reduction in miscibility may be caused by partial phase separation at low temperatures. The small but negative χ implies that the amorphous P(VDF/TrFE) and amorphous PBA phase are miscible. Any partial phase separation, if it occurs, may be of the solid–liquid type driven by crystallization rather than the liquid–liquid type because χ is expected to be positive in order for an upper critical solution temperature (UCST) to exist.

From the depolarized light scattering experiment of the PVDF/PMMA blend, Tomura et al. [2] found the existence of the UCST a few degrees below the crystallization temperatures of PVDF. In addition, their system shows a lower critical solution temperature (LCST) in the vicinity of polymer degradation temperatures. It appears that the $+\chi$ changes to the negative sign during cooling in the melt as evidenced by the melting point depression. This $-\chi$ can change its sign again below the crystallization temperatures, thus the UCST could exist in principle. Very recently, our

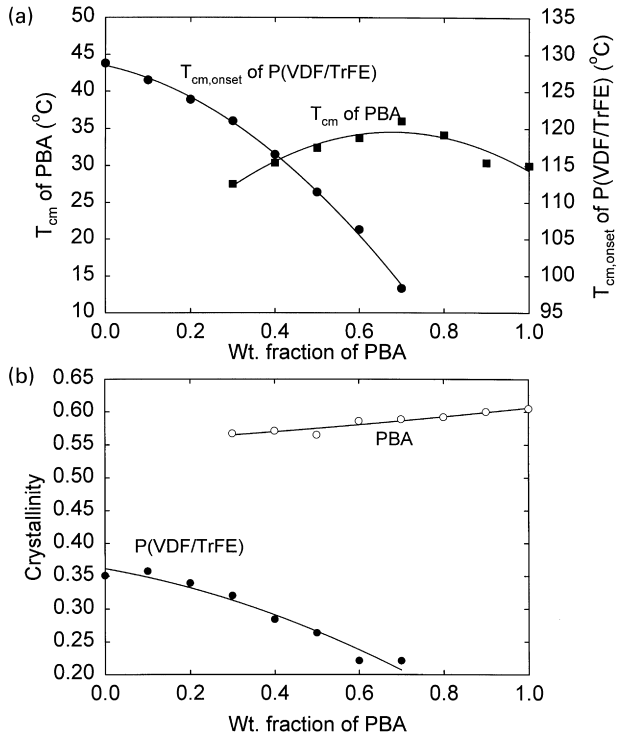

Fig. 6. Melt crystallization behavior of P(VDF/TrFE) and PBA in P(VDF/TrFE)/PBA blends showing the variation of (a) T_{cm}: peak temperature of crystallization from melt and $T_{cm,onset}$: onset temperature of crystallization from melt; and (b) crystallinity as a function of PBA wt fraction.

group also reported a possible existence of the UCST type phase separation in the temperature range of $T \ll T_m$(PVDF) for the PVDF/PBA blend in addition to the LCST in the melt [27]. One possible reconciliation is that the competition between the crystallization induced (solid–liquid) phase separation and the liquid–liquid phase separation (associated with the UCST) determine whether or not the UCST would be observable in the vicinity of crystallizing temperatures [28].

3.5. Crystallization behavior

The top and the bottom plots of Fig. 6 illustrate the melt-crystallization temperature and the normalized crystallinity of the individual components, respectively. The crystallization temperature of P(VDF/TrFE) corresponds to the onset temperature of the crystallization exotherm recorded on DSC when the blends are cooled from the melt at a cooling rate of 5°C/min. The crystallization temperature of PBA was determined from the exothermic peak. The normalized crystallinity was calculated from the melt-crystallization enthalpy of the cooling run (see the bottom of Fig. 6). It is apparent that both components can crystallize readily in the mixtures over a wide composition range. Since the crystallization temperatures of the constituents are well separated from each other and the crystallization temperature of P(VDF/TrFE) is well above the melting point of PBA, the melt-crystallization of P(VDF/TrFE) should be completed

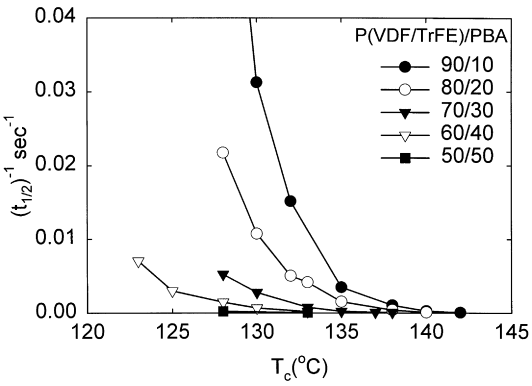

Fig. 7. Plots of $(t_{1/2})^{-1}$ versus crystallization temperature for various P(VDF/TrFE)/PBA blends.

before the crystallization of PBA begins during cooling. The crystallization of each component therefore occurs separately in the blend, rejecting amorphous materials from the crystallizing fronts. The rejected amorphous polymers are probably miscible as evidenced by a single T_g. Below the crystallization temperature of PBA, the blends have a three-phase morphology consisting of two distinct crystalline phases coexisting with a single amorphous phase.

The melt-crystallization temperature and the normalized crystallinity of P(VDF/TrFE) are rapidly reduced with increasing PBA. This can be related to the reduced rate of melt-crystallization. One can indirectly predict the reduction in the rate of crystallization from the depression of the melt-crystallization temperature. In general, the overall rate of crystallization can be estimated roughly based on the reciprocal half-crystallization time instead of using the rate constant of crystallization calculated from the Avrami plot. Fig. 7 illustrates the effect of blend composition on the overall rate of crystallization. As predicted from the shift of the crystallization temperature, it is noted that the addition of PBA slows down the overall crystallization. The retarding action in the crystallization of PVDF resulting from the addition of PBA was also reported for the PVDF/PBA system [15].

When the P(VDF/TrFE) crystallizes from the mixed melt state, the PBA melt is excluded from the crystal growth fronts of P(VDF/TrFE) such as the chain folded surface of the P(VDF/TrFE) lamellar crystals. The rejected amorphous PBA chains are likely to exist in the interlamellar, interfibrillar, and/or interspherulitic regions. Thus, the crystallization behavior of PBA with continued cooling below the crystallization temperature of PBA is expected to be appreciably different from that of P(VDF/TrFE) in the miscible mixture. From the plot of the melt-crystallization temperature of PBA, it is striking to see that the melt-crystallization temperature is shifted to higher temperatures rather than to lower temperatures with the addition of P(VDF/TrFE) in the 0/100 ∽ 30/70 composition range. This unique observation indicates that the overall crystallization of PBA in these blend composition ranges was expedited as compared with

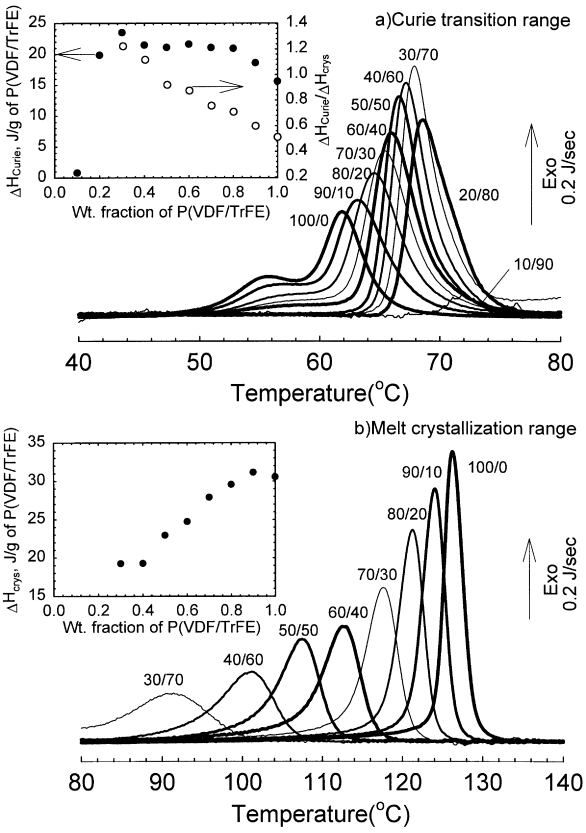

Fig. 8. The melt-crystallization and Curie transition exotherms as a function of blend composition during cooling from the melt at 5°C/min. (bottom): melt-crystallization; (top): Curie transition from the paraelectric to the ferroelectric phase.

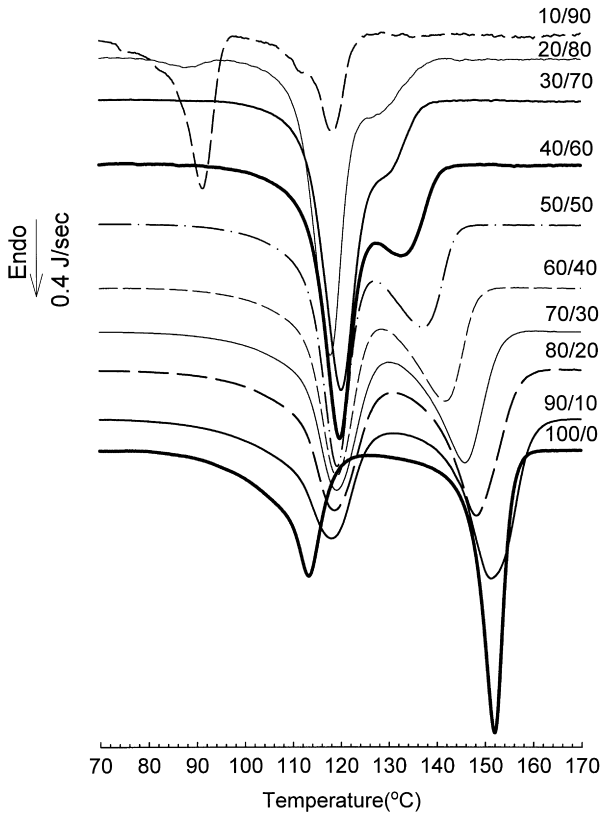

Fig. 9. Curie transition (low temperature peak) and melting endotherms (high temperature peak) as a function of blend composition upon heating the melt-crystallized samples at 20°C/min.

that in the pure PBA. Since, as mentioned earlier, the P(VDF/TrFE) phase is generally ferroelectric crystal just before the crystallization of PBA takes place, the crystallized ferroelectric P(VDF/TrFE) surface probably provides a foreign substrate for the PBA to nucleate. The heterogeneous nucleation on the P(VDF/TrFE) crystal substrate not only increases the density of PBA nuclei, but also increases the rate of nucleation with increasing P(VDF/TrFE). However, the addition of P(VDF/TrFE) can reduce the rate of crystal growth resulting from the reduced rate of diffusion caused by an increasing glass transition temperature and the dilution effect which reduces the number of crystallizable units at the crystal growth front. These effects become more prominent as the P(VDF/TrFE) composition in the blends increases, reducing the overall crystallization rate of PBA. Thus, the maximum in the crystallization temperature versus blend composition may result from the combined contributions of the enhanced nucleation rate and the retarded crystal growth rate.

3.6. Effect of PBA on Curie transition of P(VDF/TrFE)

Fig. 8 depicts the melt-crystallization and Curie transition exotherms as a function of blend composition. All of these DSC thermograms are normalized on the basis of the unit gram of P(VDF/TrFE). As pointed out earlier, the increasing PBA content shifts the crystallization curves to lower temperatures and reduces the normalized area under the curve significantly while the curves become broader. These kinds of changes may be attributed to the crystallization-retarding action of PBA. The broader melt-crystallization curve indicates that there can be a variety of paraelectric crystals with different lamellar thickness and perfection with an increasing amount of PBA. Although the Curie transition is a crystal–crystal transition occurring within the P(VDF/TrFE) crystalline phase, the miscibility of P(VDF/TrFE) with PBA can affect crystalline structures such as packing density, lamellar thickness, crystallinity, perfection, etc. thus the blend composition should have a direct influence on the Curie transition.

The DSC endothermic curves of the non-isothermally melt-crystallized sample are shown in Fig. 9. As can be seen in Fig. 8, the exotherms for the Curie transition, i.e. the paraelectric-to-ferroelectric transition, which are well resolved from the melt-crystallization exotherms of P(VDF/TrFE), are shifted to higher temperatures while showing a drastic increase in the area under the curve with the addition of PBA up to 70 wt% of PBA. On the other hand, the endotherms for the Curie transition, i.e. the ferroelectric-to-paraelectric transition, upon heating are not well resolved from the melting endotherm of

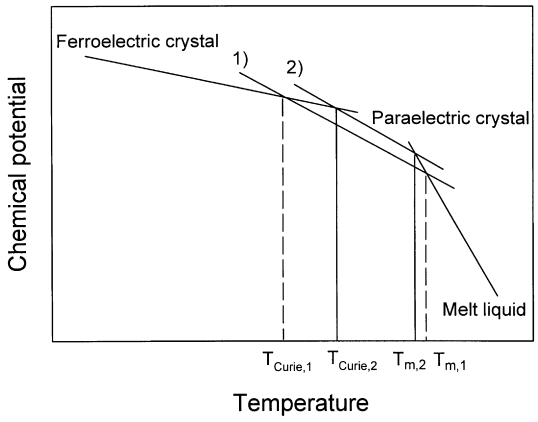

Fig. 10. Chemical potentials of the ferroelectric, paraelectric, and melting transitions of P(VDF/TrFE) as a function of temperature.

P(VDF/TrFE) in the blends (Fig. 9). Even though the shift of the ferroelectric-to-paraelectric phase transition curve is less distinct relative to that of the paraelectric-to-ferroelectric phase transition, they are shifted definitively to higher temperatures with the addition of PBA. Concurrently, the melting temperature and the melting enthalpy are significantly depressed with increasing PBA concentration as in the case of the melt-crystallization. These observed trends are the same for the heating scans as well as for the cooling runs.

The contrasting behavior of the Curie transition and the melt-crystallization resulting from the addition of PBA may be explained simply from the thermodynamic point of view as depicted in Fig. 10. The melting temperature is an intersection of two chemical potential lines (or convex curves may be more accurate, but lines are used for simplicity) representing the paraelectric crystal and the melt, respectively. Similarly, the Curie transition point can be defined as an intersection of the two chemical potential lines for each ferroelectric and paraelectric phase. The upward shift of the chemical potential line resulting from thermodynamic instability of the paraelectric phase results in the depression of the melting point, but in the elevation of the Curie transition point. With the addition of PBA, the paraelectric crystal phase becomes thermodynamically unstable, which results in the upward shift of the chemical potential line of the paraelectric phase. Consequently, the Curie transition shifts to a higher temperature while the melting point is lowered with increasing PBA concentration in the blends.

The dual Curie transitions observed in the P(VDF/TrFE)-rich blends especially upon cooling seems to support the previous thermodynamic argument. The paraelectric-to-ferroelectric phase transition at higher temperatures corresponds to the transition from the less-stable paraelectric phase to the more-stable ferroelectric phase having less gauche defects [18]. On the other hand, the paraelectric-to-ferroelectric phase transition at lower temperatures represents the transition from the more-stable paraelectric phase to the less-stable ferroelectric phase with a considerable amount of gauche defects. The peak area of the paraelectric-to-ferroelectric phase transition at the lower temperature is significantly reduced with increasing PBA concentration. This suggests that the addition of PBA decreases significantly the amount of the thermodynamically stable paraelectric crystal phase having less conformational defects because of the highly reduced rate of melt-crystallization during cooling from the melt.

It can be noticed that the ratio of the Curie transition enthalpy to the melt-crystallization enthalpy is increased nearly linearly with the amount of PBA in the blends (see the top of Fig. 8). The Curie transition enthalpy turns out to be even larger than the melt-crystallization enthalpy in the 40/60 and 30/70 blends. In the DSC curves acquired during heating of the non-isothermally melt-crystallized sample (see Fig. 9), the blends with more than 50% of PBA clearly show more pronounced Curie transition curves relative to the melting curves. This indicates that in the P(VDF/TrFE) blend, some of the ferroelectric phases, if not all, can be formed directly from the melt upon cooling or can be transformed directly to the melt without the prior formation of the paraelectric phase upon heating. Although this observation was not achieved in other P(VDF/TrFE) blend systems, the simple thermodynamic picture in Fig. 10 clearly demonstrates that the ferroelectric phase can be formed directly from the melt without forming the paraelectric phase, if the chemical potential of the paraelectric crystal continues to increase beyond the intersection of the melting and ferroelectric potentials.

4. Conclusions

The phase diagram of P(VDF/TrFE)/PBA blends showed the LCST, two melting transitions corresponding to the constituents, the Curie transitions of P(VDF/TrFE), and a single glass transition. The analysis of non-equilibrium melting points of P(VDF/TrFE) as a function of PBA concentration yielded a large negative value of $\chi_{12} = -0.592$ at 160°C. However, the interaction parameter, calculated from the melting point depression of PBA as a function of amorphous P(VDF/TrFE) concentration, was reduced to -0.071 at 61°C. This reduced miscibility (smaller negative χ at lower temperatures) is consistent with the poor miscibility indicated by the small k value of the Gordon–Taylor equation (i.e. the glass transition behavior of the blend). As evidenced by the IR band shift of the C = O absorption, the origin of the blend miscibility at elevated temperatures was attributed to the specific interaction between the carbonyl group of PBA and CF (or CF_2/CH_2) group of P(VDF/TrFE). The addition of PBA decreases the overall melt-crystallization rate of P(VDF/TrFE) resulting from the dilution effect making it more difficult for nucleation. The crystal surface of P(VDF/TrFE) provides the new substrate for PBA to nucleate. The crystallization rate of PBA increases up to 30/70

composition because of the increasing nucleation rate, thereafter the overall crystallization rate is gradually decreased resulting from the dilution effect and the reduced rate of diffusion. The addition of PBA increases the Curie transition enthalpy as well as the Curie transition temperature up to 70 wt% of PBA. The formation of some of the ferroelectric phases directly from the melt was verified experimentally in the P(VDF/TrFE/PBA) blends, particularly in the compositions rich in PBA. Based on a simple thermodynamic consideration, we have demonstrated that the ferroelectric phase can indeed be formed directly from the melt without undergoing the paraelectric phase.

Acknowledgements

One of the authors (KJK) greatly appreciates partial support from Kyung Hee University, Korea, for his sabbatical leave at the University of Akron.

References

[1] Paul DR, Barlow JW, Bernstein RE, Wahrmund DC. Polym Eng Sci 1978;18:1225.
[2] Tomura H, Saito H, Inoue T. Macromolecules 1992;25:1611.
[3] Saito H, Stühn B. Macromolecules 1994;27:216.
[4] Canalda JC, Hoffmann Th, Martinez-Salazar J. Polymer 1995;36:981.
[5] Kim KJ, Cho YJ, Kim YH. Polymer (Korea) 1994;18:502.
[6] Kim KJ, Cho YJ, Kim YH. Vibrational Spectroscopy 1995;9:147.
[7] Tanaka H, Nishi T. Phys Rev B 1986;33:32.
[8] Maiti P, Nandi AK. Polymer 1998;39:413.
[9] Kim KJ, Rho YS, Choi DH. J Korean Fiber Soc 1997;34:304.
[10] Kim KJ, Kim GB, Han SH. J Appl Polym Sci 1993;49:7.
[11] Kim KJ. unpublished.
[12] Jo WH, Park SJ, Kwon IH. Polym International 1992;29:173.
[13] Huang J, Prasad A, Marand H. Polymer 1994;35:1896.
[14] Penning JP, Manley R St J. Macromolecules 1996;29:77.
[15] Penning JP, Manley R St J. Macromolecules 1996;29:84.
[16] Fujita K, Kyu T, Manley R St J. Macromolecules 1996;29:91.
[17] Liu L-Z, Chu B, Penning JP, Manley R St J. Macromolecules 1997;30:4398.
[18] Kim KJ, Kim GB. J Appl Polym Sci 1993;47:1781.
[19] Kim KJ, Reynolds NM, Hsu SL. J Polym Sci Polym Phys Ed 1993;31:1555.
[20] Kim KJ, Kim GB, Vanlencia CL, Rabolt JF. J Polym Sci: Polym Phys Ed 1994;32:2435.
[21] Kim KJ, Kim GB. Polymer 1997;38:4881.
[22] Legrand JF, Lajzerowicz J, Berge B, Delzenne P, Macchi F, Bourgaux-Léonard C, Wicker A, Kruger JK. Ferroelectrics 1988;78:151.
[23] Tashiro K, Takano K, Kobayashi M, Chatani Y, Tadokoro H. Polymer 1981;22:1312.
[24] Nishi T, Wang TT. Macromolecules 1975;8:909.
[25] Hoffman JD, Weeks JJ. Res Natl Bur Stand A 1962;66:13.
[26] Gordon M, Taylor JS. J Appl Chem 1952;2:493.
[27] Isayeva I, Kyu T, Manley R St J. Polymer 1998;39:4599.
[28] Kim KJ, Kyu T. unpublished.